Distant homologies and domain conservation of the Hereditary Spastic Paraplegia protein SPG11/ALS5/spatacsin

Alexander L Patto and Cahir J O'Kane*

Department of Genetics, University of Cambridge, Downing Street, Cambridge, CB2 3EH

*Corresponding author Email: c.okane@gen.cam.ac.uk

Abstract

Loss-of-function mutations in SPG11 protein (spatacsin) are a common cause of autosomal recessive hereditary spastic paraplegia with thin corpus callosum. To identify regions of the protein that may have functions that are disrupted in disease, we carried out bioinformatic analyses of its conserved regions. An N-terminal region of around 650 amino-acid residues, present in SPG11 across a wide range of metazoan animals, was missing from many insect lineages. Evolutionary loss of this domain correlated with loss of its binding partner, the AP-5 adaptor complex, suggesting that its main function is interaction with AP-5 in intracellular trafficking, and that the remainder of SPG11 carries out AP-5-independent functions. At the C-terminus of SPG11, a spatacsin_C domain showed sequence similarity and predicted structural homology to the Vps16_C domain of the HOPS complex protein Vps16. It localized to acidic compartments, consistent with a role in endolysosomal or autolysosomal transport, like Vps16. Mass spectrometry analysis of binding partners of this domain identified membrane trafficking proteins, some SM proteins, and several aminoacyl-tRNA synthetases. Since mutations affecting SPG11 or aminoacyl-tRNA synthetases can both cause Charcot-Marie-Tooth neuropathy (CMT) type 2, we suggest autolysosomal trafficking as a target process in CMT type 2.

Introduction

Loss-of-function mutations in *SPG11* commonly result in autosomal recessive Hereditary Spastic Paraplegia (ARHSP) with thinning of the corpus callosum (TCC) (Stevanin *et al.* 2007). *SPG11* is the most common recessive HSP, with HSP-causing mutations identified throughout the coding region. *SPG11* mutations can also cause other degenerative disorders including juvenile ALS (Orlacchio *et al.* 2010; Daoud *et al.* 2012), juvenile Parkinson's disease and dopaminergic neuron loss (Guidubaldi *et al.* 2011; Anheim *et al.* 2009), Kjellin's syndrome, or the peripheral neuropathy Charcot-Marie-Tooth disease (Fridman and Murphy 2014; Montecchiani *et al.* 2016).

Loss of *SPG11* in mammals leads to axonal pathology, including axon outgrowth defects in mice (Pérez-Brangulí *et al.* 2014). Young *Spg11* knockout mice have severe neuronal loss in the cerebellum, motor cortex and Purkinje cells (Varga *et al.* 2015). Externally, mice develop a progressive gait disorder, developing ataxia after 12 months (Varga *et al.* 2015), similar to symptoms of *SPG11* patients (Zhao *et al.* 2013). In zebrafish, severe knockdown of *Spg11* or *Spg15* led to similar defects in spinal motor neuron axon outgrowth and locomotion difficulties (Martin *et al.* 2012). *Spg11* phenotypes in animal models and humans are broadly consistent, suggesting important roles for SPG11 in neuronal development and function.

SPG11 localizes to Lamp1-positive compartments in human fibroblasts (Hirst *et al.* 2013), which comprise lysosomes (Rohrer *et al.* 1996), autolysosomes (Yu *et al.* 2010) and late endosomes (Szymanski *et al.* 2011). SPG11 and its binding partner SPG15 show structural homology with clathrin heavy chain and COP1 subunits (Hirst *et al.* 2011; Hirst *et al.* 2013), and interact with the adaptor protein complex AP-5 (Renvoisé *et al.* 2014; Słabicki *et al.* 2010; Hirst *et al.* 2011), by binding of the SPG11 N-terminus to AP-5 (Hirst *et al.* 2013). While this is superficially similar to the recruitment of clathrin to budding vesicles by adaptors, knockdown of *AP5z1* has in fact no effect on localization of SPG11 or SPG15, and knockdown of either SPG11 or SPG15 disrupts AP-5 localization (Hirst *et al.* 2013). Loss of SPG11, SPG15 or the AP-5 subunit AP5z1 causes accumulation of the mannose 6-phosphate receptor (CIMPR) in early endosomes (Hirst *et al.* 2013), and proteomic analyses of of AP5z1 knockout cells suggest a defect in transport from late endosomes to the Golgi (Hirst *et al.* 2018). Therefore, SPG11, SPG15 and AP-5 appear to share trafficking roles that may be disrupted in HSP.

SPG11 must also have AP-5-independent roles, which may account for disease phenotypes like ALS, PD or CMT, not so far found in human AP-5 mutant genotypes. Mutations in *AP5z1* are associated with HSP, although protein null alleles appear in general to have later onset (Hirst *et al.* 2016; Słabicki *et al.* 2010) than *SPG11* or *SPG15* (Pensato *et al.* 2014; Boukhris

et al. 2008; Stevanin *et al.* 2007). Further, *Drosophila* contains both SPG11 and SPG15 homologs, but lacks AP-5 (Hirst *et al.* 2011). Such an AP-5-independent role appears to be in autophagic lysosome reformation (ALR) (Chang *et al.* 2014; Varga *et al.* 2015), which replenishes free lysosomes after periods of increased autophagy (Yu *et al.* 2010). Loss of SPG11 or SPG15 results in enlarged or excess autolysosomes, and loss of Lamp1-positive tubules on autolysosomes, thought to be an intermediate in ALR (Chang *et al.* 2014; Vantaggiato *et al.* 2013; Varga *et al.* 2015). Levels of LC3-II, an indicator of autophagy flux (Mauvezin *et al.* 2014), increase, but not Lamp1, suggesting aberrant lysosome-dependent clearance of autophagosomes (Chang *et al.* 2014; Varga *et al.* 2015). *Spg11* knock-out mice display fewer free lysosomes in Purkinje cell somata (Varga *et al.* 2015), consistent with impaired ALR *in vivo*. Mutant *SPG15* patient fibroblasts accumulate autophagy substrate p62 (Vantaggiato *et al.* 2013), and *SPG11* knock-out Purkinje cells show increased p62 in Lamp1-positive compartments, suggesting that autolysosomes are not completely functional (Varga *et al.* 2015). The above findings suggest a key role for SPG11 in ALR, and that ensuing accumulation of undegraded material in the absence of SPG11 may be a cause of neuronal degeneration (Varga *et al.* 2015).

However, the molecular role of SPG11 in autophagic trafficking, the steps it affects, and the nature of its AP-5- independent function are not clear. To identify potential roles for SPG11 in this process, we undertook bioinformatic analyses of the protein. We found that the presence or absence of the N-terminal region, found in most metazoan lineages, correlates with the presence or absence of the AP-5 adaptor complex, suggesting that the main function of the N-terminal region is to interact with AP-5. We also found evidence that the spatacsin_C domain at the C-terminus of SPG11 is homologous to the Vps16_C domain, and identified binding partners that might provide some common mechanisms for CMT pathology between SPG11 and aminoacyl-tRNA synthetases.

Materials and Methods

Amino acid alignments and protein function prediction. Multiple alignments of Spg11 sequences only were performed using Kalign multiple alignment, with gap open penalty of 13 (http://www.ebi.ac.uk/Tools/msa/kalign/) (Lassmann and Sonnhammer 2005), or MUSCLE multiple alignment (http://www.ebi.ac.uk/Tools/msa/muscle/) (Edgar 2004). Distant homologs were identified and aligned using HHpred (Zimmermann *et al.* 2018) on the MPI bioinformatic server (https://toolkit.tuebingen.mpg.de/hhpred). Tertiary structure prediction by homology was performed by submitting a multiple sequence alignment generated on the HHpred site to Modeller (Webb and Sali 2016). Interaction maps and GO and KEGG term enrichment were performed by submitting the list of *Drosophila* genes to String (http://string-db.org)

Immunoprecipitation and mass spectrometry of GFP- tagged Spg11 C-terminus. We used Gateway recombination cloning technology (Invitrogen, UK) to generate a GFP::Spg11-C-term (nucleotides 3051-4094 of *Drosophila Spg11* gene). The entry and destination vectors were pDONR211 (Thermo Fisher, 12536017), Act5-Nterm GFP tag (driven by Actin5 promoter, pAGW plasmid, https://emb.carnegiescience.edu/drosophila-gateway-vector-collection) and PMT-pcBlast-Nterm GFP tag (CuSO4 Inducible promoter, Thermo Fisher V413020).

The C-terminal region of Spg11 (amino acid residues 1468-1815) was amplified using Phusion Flash High-Fidelity polymerase (Thermo Fisher F548L) and extracted from electrophoresis gel using QIAquick Gel Extraction Kit (Qiagen 28704) according to manufacturer's protocol. The C-terminus from codons 1468-1815 was amplified using primers Spg11_C_f1 (GGGGACAAGTTTGTACAAAAAAGCAGGCTTC CAC CTG TGT TTC GTG CAC GA; forward sequence annealing to codons 1468-1473, HLCFVH shown as triplets) and Spg11_C_r1 (GGGGACCACTTTGTACAAGAAAGCTGGGTC CTA CGT ATC TCC TGC TGT GTG GA; complementary sequence annealing to codons 1810-1815 HTAGDT and stop, shown as triplets); they also contained additional homology to pDONR 211 allowing homologous recombination and integration of Spg11 C-terminus. BP and LR reactions conducted according to the Gateway® recombination cloning technology manual, and transformed into DH5-alpha cells according to the manufacturers instructions (Subcloning efficiency, ThermoFisher 18265017). Clones were sequenced (GATC-Biotech) using M13f and M13r primers, to ensure sequences were correct.

Transfection of *Drosophila* Mel-2 Cells. *Drosophila* Mel-2 cells (Schneider 1972) were grown at 25°C in standard sterile cell flasks in Express SFM medium (LifeTechnologies), containing penicillin streptomycin (ThermoFisher) and L-glutamine (ThermoFisher). All cell

work was carried out in a sterile hood. Prior to transfection, cells were grown to high confluence and seeded in 2 ml Express SFM (LifeTechnologies) in a 6-well plate, then left for 2 hours. To transform Mel-2 cells with GFP-tagged Spg11 C-terminus, 3 µg of plasmid DNA was diluted in 100 µl ddH_2O in a microfuge tube. A helper plasmid (0.5 µg) was added in parallel with Act5-Nterm GFP tag to confer Mel-2 cells with blasticidin resistance. Next, 15 µl of FuGene-HD transfection reagent (Promega E2311) was applied directly to the center of the microfuge tube, and mixed thoroughly by gently pipetting up and down, before incubation for 15 minutes to allow formation of transfection complexes. Transfection mixture was added to the cells slowly, and the cell culture was subsequently incubated at 25°C for 12 hours.

Expression of GFP-tagged Spg11 C-terminus was confirmed by confocal microscopy. Mel-2 cells were seeded on sterile glass cover slips for 20 minutes, before fixing in ice cold methanol for 10 minutes. When necessary, cells were exposed to Lysotracker® for 10 minutes prior to fixation. Cells were mounted on glass slides before imaging.

Transfected Mel-2 cells were selected using blasticidin (ThermoFisher, USA, A1113903) for 5 passages. Cells were passaged when confluence approached 80%. They were then expanded to $7x10^8$ in 300 ml of Express SFM medium, in large sterile conical flasks, shaken at 80 rpm at 25°C. Transgene expression was induced 24 hours prior to protein extraction by adding 500 µM $CuSO_4$. The PMT-pcBlast-Nterm GFP tag, lacking Spg11, was used as a control.

***Drosophila* Mel-2 cell immunoprecipitation.** *Drosophila* Mel-2 cells were transferred into 50 ml falcon tubes and pelleted at 5000 rpm, before resuspending cells in 8 ml of RIPA buffer (Sigma R0278), containing protease inhibitors (Sigma). Cells were lysed on ice using electronic homogenizer, 5 times, each for 30 seconds, with 30 seconds cool down time in between. Lysed cells were centrifuged for 30 minutes at 10,000 rpm at 4°C, before supernatant was collected. For immunoprecipitation, ChromoTek GFP-Trap A (ChromoTek gta-10, Germany) was used according to manufacturer's instructions. GFP-tagged Spg11 C-terminus-bound beads were sent to for mass spectrometry analysis at the Mass Spectrometry Laboratory, Institute of Biochemistry and Biophysics, PAS. Poland.

Data reporting. No institutional ethical review was required. The study was not pre-registered. Randomization, blinding, and sample size calculations were not applicable. No animals were used. The study was exploratory. Statistical calculations were all carried out by the bioinformatic software described. Clones can be provided on request, or generated from the information provided in the paper.

Results

N-terminal AP-5-binding region of SPG11 is absent in insect lineages. We used bioinformatic tools to identify potential functional domains within SPG11. Multiple alignments show extensive conservation along the length of SPG11 proteins, but with no identifiable domains of known function (Hirst *et al.* 2011; Hirst *et al.* 2013). The best characterized molecular function is a predicted beta-propeller-like fold in the N-terminal 500 amino-acid residues of human SPG11, which interacts with the AP-5 adaptor (Hirst *et al.* 2013). Multiple alignment (Lassmann and Sonnhammer 2005) identified this region in all deuterostomes aligned (Fig. 1), and in many protostomes, including arachnids, molluscs, annelids and brachiopods. However, *Drosophila* and other insects lack approximately 650 amino acids from the N-terminus of SPG11 (known as CG13531 in *Drosophila*), which contains the AP-5-binding domain (Fig. 1).

AP-5 is an ancient adaptor complex, but has frequently been lost during eukaryote evolution. To test whether its loss correlates with loss of the SPG11 N-terminus, we tested a range of metazoans for the presence of any of the four AP-5 subunits (Hirst *et al.* 2011). AP-5 is present in basal animal phyla such as *Cnidaria*, the sponge *Amphimedon*, and the Placozoan *Trichoplax*; it is also found widely in deuterostomes (Figs S1-S4). In protostomes, it is found in molluscs (*Octopus*, *Lottia, Crassostrea, Biomphalaria*), the brachiopod *Lingula*, the annelid *Capitella*, the priapulid worm *Priapulus*, and some arthropods (*Limulus*, *Parasteatoda*), but not in insects. Most organisms that lack the SPG11 N-terminal region (Figure 1) also lack AP-5 (Figs S1-S4), suggesting that the primary role of the N-terminus of SPG11 is to bind AP-5.

In a few species, we found an SPG11 N-terminal domain, but not AP-5: the arthropods *Sarcoptes* and *Metaseiulus*, and the mollusc *Aplysia* (Figure 1). However, the arthropods most closely related to *Sarcoptes* and *Metaseiulus* (*Limulus*, *Parasteatoda*), and other molluscs (*Octopus*, *Lottia*), possess both AP-5 and the SPG11 N-terminus, suggesting either that AP-5 is present in *Sarcoptes*, *Metaseiulus* and *Aplysia* but not yet annotated, or these species have lost AP-5 relatively recently, but not yet the SPG11 N-terminus.

SPG11 C-terminus has predicted homology with the Vps33-binding domain of Vps16. Human and *Drosophila* SPG11 share 16% identity across the entire protein sequence, with higher identity (31%) across a C-terminal region of around 300 amino acid residues (Fig. 2A). This region is designated as a Spatacsin_C domain (Pfam 14649; Interpro IPR028107), but its function or structure is unknown. To identify domains homologous to this region of SPG11, we used *Drosophila* and human SPG11 C-terminal domain sequences as queries in a HHpred search; this search can identify distant homologies between proteins using the Structural

Classification of Proteins database (SCOP) (Söding *et al.* 2005), and previously predicted a beta-propeller-like region in the N-terminal AP-5-binding domain (Hirst *et al.* 2013). It also predicts homology of some regions of *Drosophila* SPG11 to coatomer subunits (Figure 2B), as previously predicted for human SPG11. At the C-terminus, HHpred predicted homology across most of the C-terminal 300 amino acid residues, to PDB crystal structure 4KMO (DOI 10.2210/pdb4kmo/pdb), comprising the Vps33-Vps16 HOPS subcomplex (Figure 2B,C), which contains the C-terminal region of Vps16 (Vps16_C, Pfam ID: PF04840) and the SM protein Vps33 (Baker *et al.* 2013; Graham *et al.* 2013).

Fig. 1

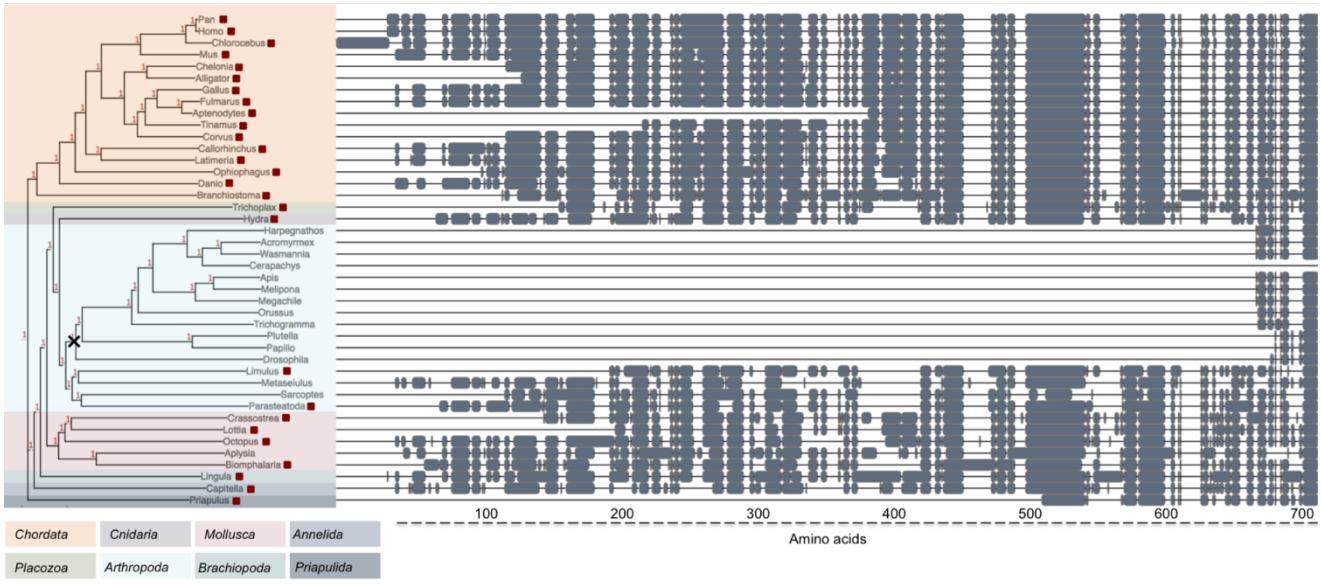

Fig. 1. SPG11 phylogenetic tree across a range of metazoans. Left: Phylogenetic tree of SPG11 amino acid sequence, made using Kalign multiple alignment (Lassmann and Sonnhammer 2005). Organisms containing AP-5 (Figs S1-S4) are shown by red squares. Shaded regions denote different phyla. Right: A condensed overview of aligned SPG11 N-terminal regions, created using online tree viewer (http://etetoolkit.org/treeview/). Predicted loss of N-terminal region occurs prior to the divergence of insects (cross).

Fig. 2

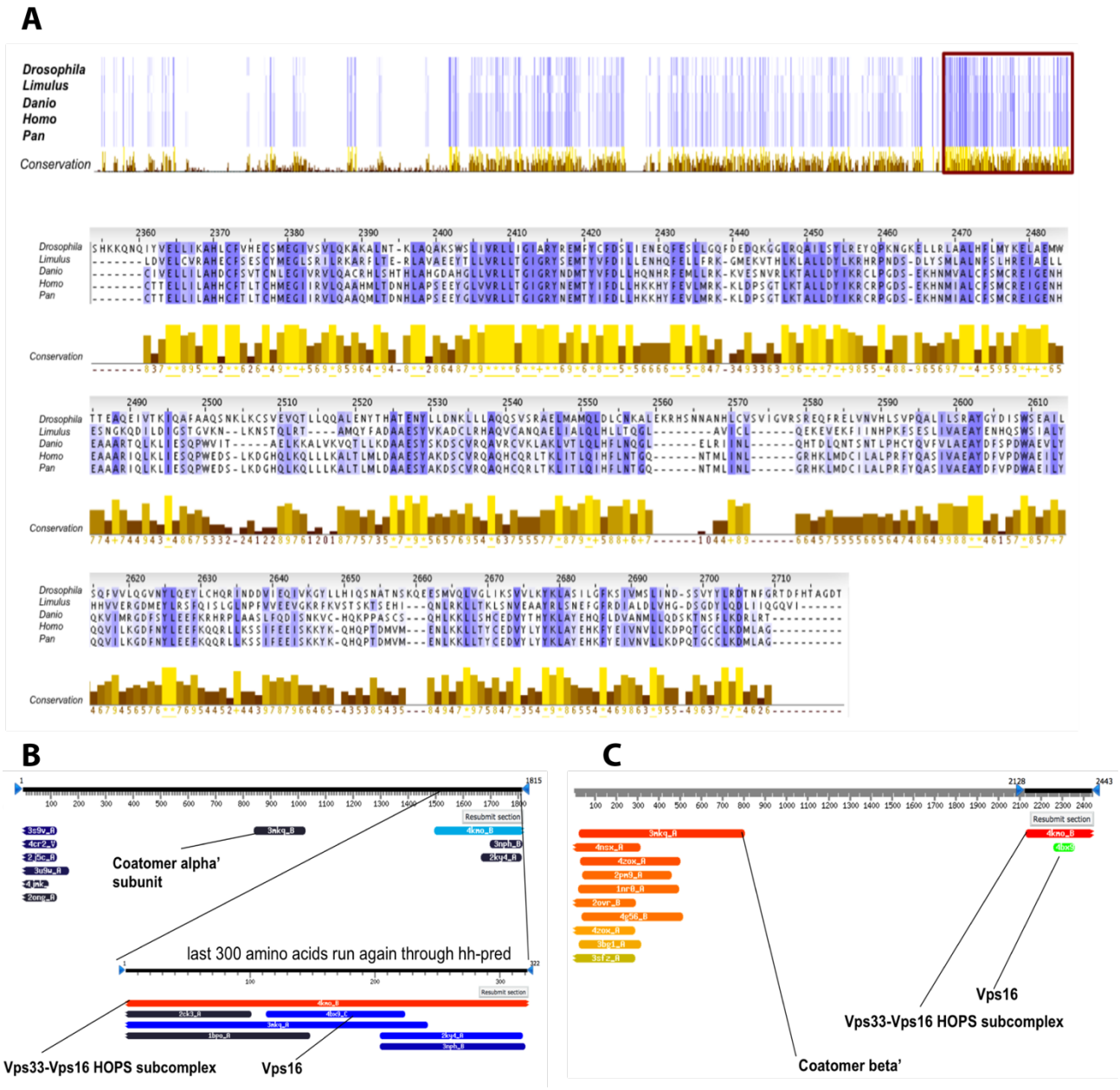

Fig. 2. Sequence conservation across the length of Spg11. A. MUSCLE multiple alignment of SPG11 from *D. melanogaster*, *L. polyphemus*, *D. rerio*, *H. sapiens* and *P. troglodytes*, shown in Jalview. Top panel: blue shaded regions show regions of amino acid identity between organisms; intensity of blue corresponds with level of identity. Yellow bars at the bottom denote conservation level between organisms for individual amino acid positions. Red box indicates SPG11 C-terminal region with high conservation. This region is expanded in the lower panels to show conservation and alignment of amino acid sequences. **B:** HHpred of *Drosophila* SPG11 predicts coatomer homology in the central region of the proteins, and homology to Vps33-Vps16 HOPS subcomplex and Vps16 in the C-terminal region. **C:** HHpred analysis of human SPG11 predicts extended homology to coatomer beta' subunit at the N-terminus and to Vps33-Vps16 HOPS subcomplex and Vps16 at the C-terminus.

To verify the sequence conservation of the SPG11 C-terminus to the Vps33-Vps16 subcomplex, we used six phylogenetically diverse SPG11 C-terminal domains as a single query in a HHpred alignment. After other Spg11 C-termini, the next most closely related sequences were the C-terminal domains of the Vps16a and Vps16b families (Supplementary Fig. 5). A multiple sequence alignment in HHpred using a small number of Spg11, Vps16A and Vps16B proteins, found extensive similarity between all three families of proteins, with identical or conserved amino acid residues at many positions (Figure 3A). However, many known Vps33-binding residues of the Vps16_C domain of Vps16 (Baker *et al.* 2013; Graham *et al.* 2013) were either missing or not conserved in SPG11 (Figure 3A). Together these results support homology of the SPG11 C-terminal domain to Vps16_C, but do not strongly support binding to Vps33.

SPG11 C-terminus predicted tertiary structure similar to Vps16_C. The Vps16_C domain forms an alpha-solenoid with 17 alpha-helices; it binds to all 3 domains of Vps33, arching around Vps33, its N-terminal region lying in a groove between Vps33 domains 1 and 2 (Baker *et al.* 2013; Graham *et al.* 2013). We assessed whether the SPG11 C-terminus might adopt a similar structure to Vps16_C, using Modeller tertiary structure prediction (Webb and Sali 2016). To give more weight to conserved residues for modeling, we tested the multiple alignment of six Spg11 sequences (Supplementary Fig. S5) for predicted similarity to the tertiary structure of Vps16_C (4KMO:B, https://www.rcsb.org/). This analysis predicted an extensive alpha-helical structure for the Spg11 C-terminus, with the majority of helices at positions compatible with those in Vps16_C (Fig. 3B). The potential of the Spg11 C-terminus to adopt a tertiary structure like Vps16_C further supports a model of its origin as a distant homolog of Vps16_C.

Fig. 3. SPG11 C-terminus shows conservation with Vps16_C domains.

A. Multiple alignment of Spg11 C-terminus with sequences from two Vps16A and two Vps16B subfamily members, grouped by color. We generated a multiple sequence alignment in HHpred (Zimmermann *et al.* 2018), exported to JALview, and made minor adjustments manually. Asterisks below alignment show residues that mostly conserved, or show only conservative changes, between the Spg11 sequences and at least one of the Vps16 sequences. Gray boxes below alignment denote Vps33-binding residues in Vps16a (Baker *et al.* 2013; Graham *et al.* 2013).

B. Tertiary structure prediction of SPG11_C was performed by forwarding a HHpred multiple sequence alignment of six Spg11_C domains from the HHpred site to Modeller (Webb and Sali 2016), to align with the tertiary structure of Vps16_C (4KMO:B, https://www.rcsb.org/). Stereo pairs show actual structure of Vps16_C and predicted structure of Spg11_C, either alone (left pairs, overlaid in top row, singly in lower rows), or bound to Vps33a (right pairs).

Figure 3

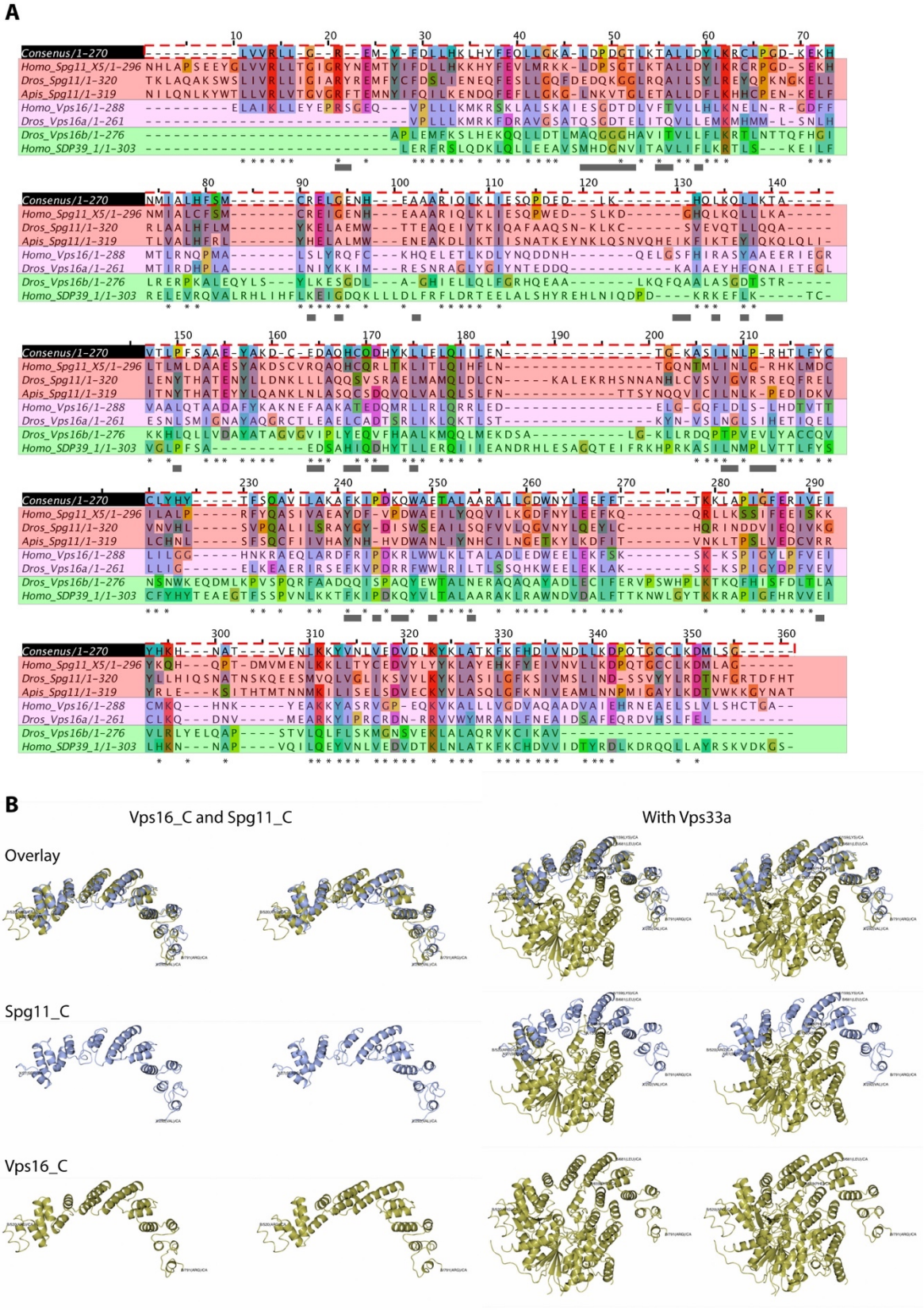
A
Consensus/1-270
Homo_Spg11_X5/1-296
Dros_Spg11/1-320
Apis_Spg11/1-319
Homo_Vps16/1-288
Dros_Vps16a/1-261
Dros_Vps16b/1-276
Homo_SDP39_1/1-303
B
Vps16_C and Spg11_C
With Vps33a
Overlay
Spg11_C
Vps16_C

GFP-tagged SGP11 C-terminus overlaps with acidic compartments. To investigate whether the SPG11 C-terminus localized to endo/auto/lysosomal compartments like Vps16 (Kim *et al.* 2001; Schröder *et al.* 2007; Wartosch *et al.* 2015) and Spg11 (Hirst *et al.* 2012; Murmu *et al.* 2011; Varga *et al.* 2015), we expressed GFP::Spg11-C (amino acid residues 1468-1815) in *Drosophila* Mel-2 cells. GFP::Spg11-C localized widely through the cytosol, but was often concentrated in puncta that overlapped with acidic LysoTracker®-positive compartments in many cells (Figure 4), showing that much of it localized to endo/auto/lysosomal compartments.

Fig. 4

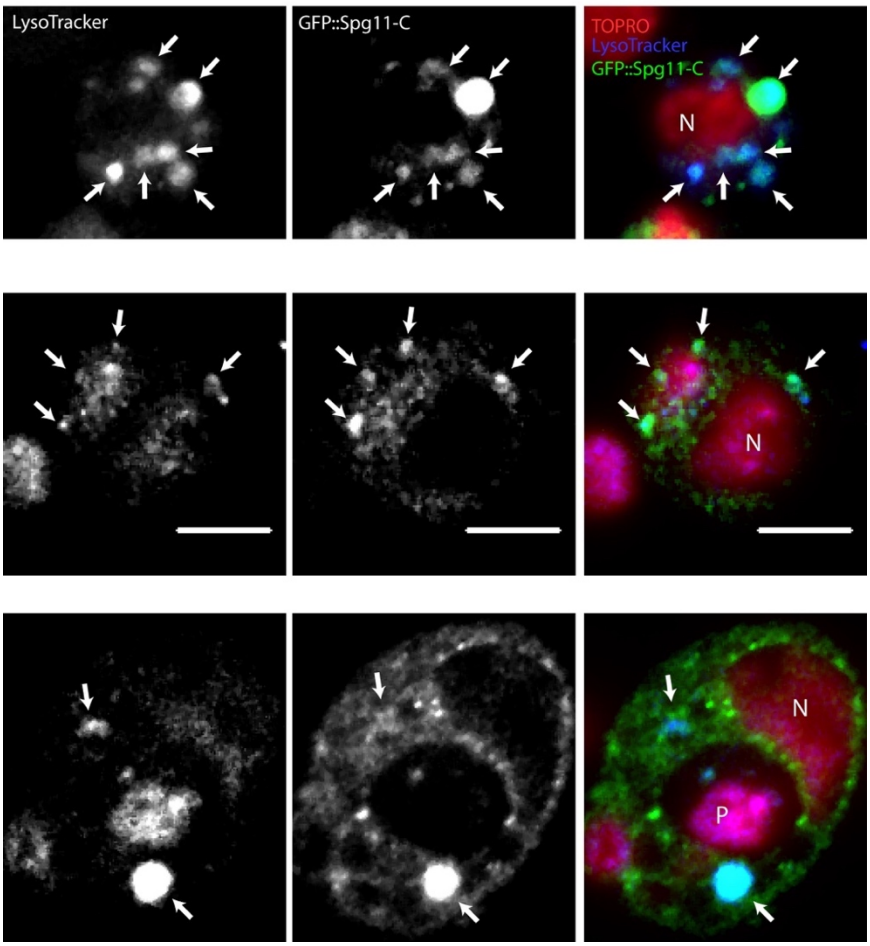

Fig. 4. Localisation of GFP::Spg11-C in *Drosophila* Dmel-2 cells. Single sections of three different transfected cells, showing overlap of many GFP::Spg11-C puncta with LysoTracker® -positive acidic compartments (examples shown by arrows). Nuclei (N) are stained lightly with TOPRO-3. One likely phaogosome (P) is visible. Scale bar = 5 µm.

Identification of SPG11 C-terminus binding partners by mass spectrometry. To test further the functionality of the SPG11 C-terminus, we conducted mass spectrometry analysis on *Drosophila* GFP::Spg11-C expressed in Mel-2 cells. We established two cell lines: one with GFP::Spg11-C driven by a constitutively active promoter (Act5-GFP::Spg11-C) and one by a $CuSO_4$-inducible promoter (PMT-GFP::Spg11-C). A Mel-2 cell line expressing GFP (inducible by $CuSO_4$) was used as a negative control.

Mass spectrometry analysis of purified GFP::Spg11-C from $CuSO_4$-induced cells identified 898 proteins not found in the GFP negative control, whereas analysis of constitutively expressed GFP::Spg11-C identified 231 proteins (Fig. 5A); the top 100 hits from each analysis are listed in Tables 1 and 2. The $CuSO_4$-induced cells generated more protein hits that showed higher scores than in the control cell line, compared to the constitutive cells (Figure 5B), suggesting that GFP::Spg11-C was more highly expressed in $CuSO_4$-inducible than in constitutive cells. 128 proteins were detected in both lines (Fig. 5A; Table 3), providing increased confidence in the specificity of these interactors, although this overlapping list may be missing some genuine interactors identified in the $CuSO_4$-induced cells.

GFP::Spg11-C was detected in both cell lines, but not in the GFP negative control line, confirming its expression, and the mass spectrometry protocol (Figure 5B); it was the highest scoring hit in the $CuSO_4$-induced line, but not in the constitutively expressing cell line (Figure 5B). Reassuringly, the SPG11 binding partner, SPG15, was identified in the inducible cell line, although not in the constitutive one. To assess the potential biological roles of Spg11, we tested for enrichment of molecular function, biological process, and pathway terms among the interactors identified in both cell lines. Membrane traffic and organization terms were among those most enriched (Table 4; Fig. 6). We also noticed several actin-binding proteins, and motor proteins of the kinesin, dynein and myosin families (Tables 1-3, entries in bold; Fig. 6).

One unexpected class of SPG11-C binding partners were aminoacyl-tRNA synthetases, which charge specific tRNAs with the correct amino acid for translation. These were the highest ranking class of interactors with a specific enzymatic activity as a molecular function, and the highest ranking KEGG pathway (Table 4). Five of these were pulled down (Figure 6; Table 5). These included *Drosophila* homologs of methionyl-tRNA synthetase (MARS) and alanyl-tRNA synthetase (AARS), mutations in which are causative for Charcot-Marie-Tooth (CMT) Type 2 neuropathy (McLaughlin *et al.* 2012; Gonzalez *et al.* 2013; Timmerman *et al.* 2014; Wei *et al.* 2019), as well as serine- valine- and glutamine- tRNA synthetases (Table 5). The MARS ortholog was identified with a particularly high score in the inducible line (Table 1).

Fig. 5

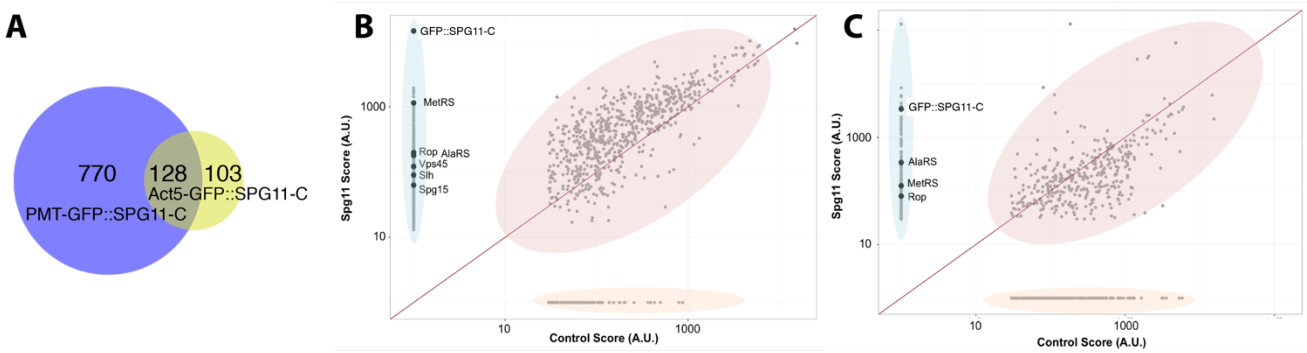

Fig. 5. Binding partners of Spg11_C identified by mass spectrometry. A. Venn diagram of Spg11_C interactors identified by mass spectrometry of PMT- GFP::Spg11-C and Act5-GFP::Spg11-C cell lines. **B,C.** Mass spectrometry output for purified GFP::Spg11-C from the *Drosophila* Mel-2 cell line expressing PMT-GFP::Spg11-C (**B**) or Act5-GFP::Spg11-C (**C**), compared to control cells lacking GFP::Spg11-C. Graphs plot the percentage difference between test and control. **B** has more proteins with a higher score than the equivalent protein in the negative GFP control, indicated by the majority of the protein hits residing above the equivalence line (in red). However, graph C has fewer proteins above the equivalence line. Scores of GFP::Spg11-C, Rop, Vps45, Slh, MetRS (MARS), AlaRS (AARS) and Spg15 are highlighted.

Fig. 6

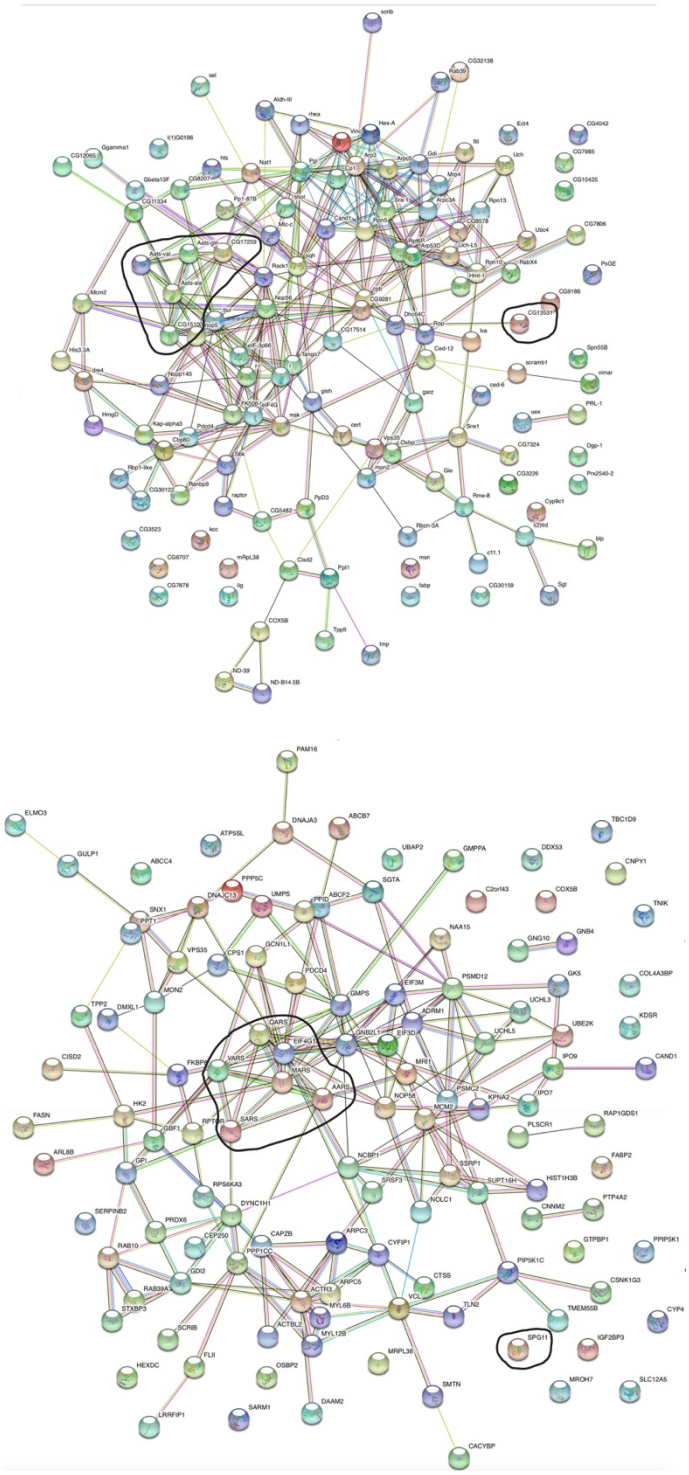

Fig. 6. Interactions among Spg11_C binding partners found in both cell lines. Top: *Drosophila* Spg11_C partners. Bottom: human orthologs of *Drosophila* Spg11_C partners. Maps were generated using String (http://string-db.org). Aminoacyl-tRNA synthetases (including CG17259/SerRS and CG15100/MetRS) are grouped inside a freehand line; human EIF4G1 is an unrelated "bystander". *Drosophila* and human CG13531/SPG11 are highlighted.

Since the Vps16_C domain of Vps16 recruits the SM proteins Vps33a to the HOPS complex (Wartosch *et al.* 2015), we expected to find one or more SM proteins as binding partners of the spatacsin_C domain. *Drosophila* has 5 known SM proteins (Table 6). Three of these, Rop, Vps45 and Slh were identified in the output of the $CuSO_4$-induced line (Figure 5B; Table 7). Rop was identified in both cell lines (Figure 5B; Table 3); we did not identify Vps33a (Carnation) or Vps33b as binding partners in either line.

Discussion

Bioinformatic analyses predict functional roles of the N- and C-termini of SPG11. Our bioinformatic analyses make interesting predictions about two regions of the SPG11 protein family. First, our phylogenetic analyses show that the evolutionary presence of a conserved N-terminal region correlates strongly with the presence of the AP-5 adaptor complex, suggesting that binding to AP-5 is the only essential function of this N-terminal region. Second, the SPG11 C-terminus shows higher conservation than most other parts of SPG11, and both human and fly variants show predicted structural homology with the Vps16 C-terminus (Vps16_C, Pfam ID: PF04840) (Figure 2C). The model of homology is supported by many conserved residues in a multiple sequence alignment of spatacsin_C and Vps16_C domains (Figure 3A) and tertiary structure prediction by homology (Figure 3B).

The Vps16_C domain (Pfam ID: PF04840) mediates binding to Vps33 proteins (Baker *et al.* 2013; Graham *et al.* 2013). These belong to the Sec1/Munc18 (SM) protein family (Misura *et al.* 2000; Graham *et al.* 2013) and have three domains, arranged in an arch-like structure, with an internal cavity capable of binding to SNARE proteins (Misura *et al.* 2000; Baker *et al.* 2013; Toonen and Verhage 2003; Baker *et al.* 2015). SM proteins bind to SNARE proteins such as syntaxin and are important for membrane fusion in disparate pathways, including synapse neurotransmitter release (Wu *et al.* 1998; Harrison *et al.* 1994; Weimer and Richmond 2004), early endosomal tracking (Nielsen *et al.* 2000) (Morrison *et al.* 2008) and Golgi-ER tracking (Laufman *et al.* 2009). However, their precise role is not fully understood.

Humans and flies have two Vps16 proteins: Vps16a, which binds to Vps33a in the HOPS and CORVET complexes that promote fusion of endosomes or autophagosome to lysosomes (Bröcker *et al.* 2012; Urban *et al.* 2012; Solinger and Spang 2013), and Vps16b, which binds to Vps33b in the analogous but smaller CHEVI complex (Hunter *et al.* 2018; van der Beek *et*

al. 2019). Therefore, the Spg11-C-terminal domain could potentially also bind to SM proteins; its divergence from known Vps16_C domains, and the relatively low conservation of Vps16 residues that bind to Vps33a, suggest that it is unlikely to bind to Vps33a or Vps33b, but it could potentially bind to other SM family proteins. The localization of the Spg11 C-terminus to acidic compartments (Figure 4A) could indicate a role for the Spg11-C-terminus in regulating some membrane fusion event(s) involving late endosomes, autophagosomes, autolysosomes, or lysosomes.

SPG11 C-terminus interacts with SM proteins Rop, Slh and Vps45. Mass spectrometry analysis of the SPG11 C-terminus expressed in *Drosophila* Mel-2 cells was used to identify potential binding partners of the Spg11 C-terminus. This identified three of the five *Drosophila* SM proteins: Rop, Slh and Vps45, which were not found in the negative GFP control, tentatively indicating that the Spg11 C-terminus may possess SM protein binding ability.

Of the SM proteins identified, Rop was the highest scoring (Table 7). Rop is the homologue of yeast Sec1p (Wu *et al.* 1998), and is involved in synaptic vesicle exocytosis, synapse transmission and secretion (Wu *et al.* 1998; Harrison *et al.* 1994; Weimer and Richmond 2004); it does not appear to bind to Vps16a or Vps16b in *Drosophila* (Pulipparacharuvil *et al.* 2005). Vps45 is important in the endocytic pathway (Nielsen *et al.* 2000; Morrison *et al.* 2008). In both humans and flies, Vps45 is part of a complex with Rab5 and a FYVE-containing protein, Rabenosyn-5, to mediate vesicle fusion to form early endosomes (Nielsen *et al.* 2000; Morrison *et al.* 2008). In humans *VPS45* mutations are associated with congenital neutropenia, with human *VPS45* patients lacking lysosomes (Stepensky *et al.* 2013). Slh is the orthologue of yeast Sly1 (Toonen and Verhage 2003). In mammals, Sly1 is implicated in Golgi-to-ER retrograde transport (Laufman *et al.* 2009; Nogueira *et al.* 2014). At this stage we cannot tell whether the SM protein interactions of the Spatacsin_C domain are direct, or of functional biological significance. However, they do occur in a native *Drosophila* cellular environment, and they are therefore consistent with the model of a Vps16_C-like function for the Spatacsin_C domain.

The Spg11 C-terminus interacts with aminoacyl tRNA synthetases. Mass spectrometry of GFP::Spg11-C pulled down five aminoacyl-tRNA (aa-tRNA) synthetases (Figure 6A), The aa-tRNA synthetases are essential for normal protein translation, by attaching the correct amino acid onto cognate tRNA molecules (Cusack 1997; Wallen and Antonellis 2013; Datta *et al.* 2009; Swairjo *et al.* 2004). However, mutations in at least two human aa-tRNA synthetases identified here, *MARS* and *AARS*, cause the axonal neuropathy, dominant Charcot-Marie-Tooth disease, type 2 (McLaughlin *et al.* 2012; Timmerman *et al.* 2014); furthermore, loss-of-

function mutations in *SPG11* (Montecchiani *et al.* 2016); as well as mutations in the Spg11 binding partner, Rab7 (Gillingham *et al.* 2014), can cause CMT type 2 (Cogli *et al.* 2009). Therefore, mutations affecting SPG11, Rab7, and aa-tRNA synthetases might cause Charcot-Marie-Tooth disease by a common mechanism.

What kind of common mechanism could this be? CMT2 causality of aa-tRNA synthetases is a dominant trait that may be due to exposure of an internal surface by CMT2 mutations, and is independent of their enzymatic activity (Blocquel *et al.* 2017); the resulting dominant neurological CMT2 disease phenotype resembles an SPG11 recessive phenotype, suggesting that either SPG11 protein or aa-tRNA synthetases might antagonize each other. Aminoacyl tRNA synthetases have functions beyond translation, including amino acid sensing and autophagy regulation, by mediating mTOR activation (Han *et al.* 2012; Bonfils *et al.* 2012; Jewell *et al.* 2013). Further, when HeLa cells are treated with Leucine, LARS translocates to the lysosomal membrane where it acts as a GTPase-activating protein (GAP) for Rag GTPase (Han *et al.* 2012; Bonfils *et al.* 2012). Since SPG11 functions on autolysosomes to regenerate lysosomes, it could interact with aa-tRNA synthetases there. We therefore hypothesize that CMT2 pathology could be caused by defects in autophagosomal lysosome reformation as occurs in SPG11 loss-of-function (Varga *et al.* 2015), or by defects in lysosomal amino-acid-sensing machinery caused by gain-of-function mutations in aminoacyl-tRNA synthetases.

Conclusions. Our analyses suggest that the sole essential function of the N-terminus of SPG11 is to bind the AP-5 adaptor complex, and support the model that its C-terminal spatacsin_C domain is a distantly related Vps_C domain, with roles in membrane trafficking. The recovery of several aminoacyl-tRNA synthetases as binding partners of this domain, suggests the possibility that mutations in human SPG11 or in aminoacyl-tRNA synthetases could give rise to Charcot-Marie-Tooth axonopathy by affecting a common cellular process in membrane trafficking.

Acknowledgements. We thank Yuu Kimata and his group for help with *Drosophila* cell culture and establishment of cell lines, and the *Drosophila* Genomics Resource Center (supported by NIH Grant 2P40OD010949) for plasmids. This work was funded by a PhD studentship 861-792 from the UK Motor Neuron Disease Association and the Le Bouedec family to ALP, and by a grant from the Tom-Wahlig Stiftung to CJO'K.

References

Anheim M., Lagier-Tourenne C., Stevanin G., Fleury M., Durr A., Namer I. J., Denora P., et al. (2009) SPG11 spastic paraplegia: A new cause of juvenile parkinsonism. *J. Neurol.* **256**, 104–108.

Baker R. W., Jeffrey P. D., Hughson F. M. (2013) Crystal Structures of the Sec1/Munc18 (SM) Protein Vps33, Alone and Bound to the Homotypic Fusion and Vacuolar Protein Sorting (HOPS) Subunit Vps16*. *PLoS One* **8**.

Baker R. W., Jeffrey P. D., Zick M., Phillips B. P., Wickner W. T., Hughson F. M. (2015) A direct role for the Sec1/Munc18-family protein Vps33 as a template for SNARE assembly. *Science (80-.).* **349**, 1111–1114.

Beek J. van der, Jonker C., Welle R. van der, Liv N., Klumperman J. (2019) *CORVET, CHEVI and HOPS – Multisubunit tethers of the endo-lysosomal system in health and disease*.

Blocquel D., Li S., Wei N., Daub H., Sajish M., Erfurth M. L., Kooi G., et al. (2017) Alternative stable conformation capable of protein misinteraction links tRNA synthetase to peripheral neuropathy. *Nucleic Acids Res.* **45**, 8091–8104.

Bonfils G., Jaquenoud M., Bontron S., Ostrowicz C., Ungermann C., Virgilio C. De (2012) Leucyl-tRNA Synthetase Controls TORC1 via the EGO Complex. *Mol. Cell* **46**, 105–110.

Boukhris A., Stevanin G., Feki I., Denis E., Elleuch N., Miladi M. I., Truchetto J., et al. (2008) Hereditary spastic paraplegia with mental impairment and thin corpus callosum in Tunisia: SPG11, SPG15, and further genetic heterogeneity. *Arch. Neurol.* **65**, 393–402.

Bröcker C., Kuhlee A., Gatsogiannis C., Kleine Balderhaar H. J., Hönscher C., Engelbrecht-Vandré S., Ungermann C., Raunser S. (2012) Molecular architecture of the multisubunit homotypic fusion and vacuole protein sorting (HOPS) tethering complex. *Proc. Natl. Acad. Sci. U. S. A.* **109**, 1991–1996.

Chang J., Lee S., Blackstone C. (2014) Spastic paraplegia proteins spastizin and spatacsin mediate autophagic lysosome reformation. *J. Clin. Invest.* **124**, 5249–5262.

Cogli L., Piro F., Bucci C. (2009) Rab7 and the CMT2B disease, in *Biochem. Soc. Trans.*, Vol. 37, pp. 1027–1031.

Cusack S. (1997) Aminoacyl-tRNA synthetases. *Curr. Opin. Struct. Biol.* **7**, 881–889.

Daoud H., Zhou S., Noreau A., Sabbagh M., Belzil V., Dionne-Laporte A., Tranchant C., Dion P., Rouleau G. A. (2012) Exome sequencing reveals SPG11 mutations causing juvenile ALS. *Neurobiol. Aging* **33**, 839.e5-839.e9.

Datta D., Vaidehi N., Zhang D., Goddard W. A. (2009) Selectivity and specificity of substrate binding in methionyl-tRNA synthetase. *Protein Sci.* **13**, 2693–2705.

Edgar R. C. (2004) MUSCLE: Multiple sequence alignment with high accuracy and high throughput. *Nucleic Acids Res.* **32**, 1792–1797.

Fridman V., Murphy S. M. (2014) *The spectrum of axonopathies: From CMT2 to HSP*.

Gillingham A. K., Sinka R., Torres I. L., Lilley K. S., Munro S. (2014) Toward a Comprehensive Map of the Effectors of Rab GTPases. *Dev. Cell* **31**, 358.

Gonzalez M., McLaughlin H., Houlden H., Guo M., Liu Y. T., Hadjivassilious M., Speziani F., et al. (2013) Exome sequencing identifies a significant variant in methionyl-tRNA synthetase (MARS) in a family with late-onset CMT2. *J. Neurol. Neurosurg. Psychiatry* **84**, 1247–1249.

Graham S. C., Wartosch L., Gray S. R., Scourfield E. J., Deane J. E., Luzio J. P., Owen D. J.

(2013) Structural basis of Vps33A recruitment to the human HOPS complex by Vps16. *Proc. Natl. Acad. Sci. U. S. A.* **110**, 13345–13350.

Guidubaldi A., Piano C., Santorelli F. M., Silvestri G., Petracca M., Tessa A., Bentivoglio A. R. (2011) Novel mutations in SPG11 cause hereditary spastic paraplegia associated with early-onset levodopa-responsive Parkinsonism. *Mov. Disord.* **26**, 553–556.

Han J. M., Jeong S. J., Park M. C., Kim G., Kwon N. H., Kim H. K., Ha S. H., Ryu S. H., Kim S. (2012) Leucyl-tRNA synthetase is an intracellular leucine sensor for the mTORC1-signaling pathway. *Cell* **149**, 410–424.

Harrison S. D., Broadie K., Goor J. van de, Rubin G. M. (1994) Mutations in the drosophila Rop gene suggest a function in general secretion and synaptic transmission. *Neuron* **13**, 555–566.

Hirst J., Barlow L., Francisco G. C., Sahlender D. A., Seaman M. N. J., Dacks J. B., Robinson M. S. (2011) The fifth adaptor protein complex. *PLoS Biol.* **9**.

Hirst J., Borner G. H. H., Antrobus R., Peden A. A., Hodson N. A., Sahlender D. A., Robinson M. S. (2012) Distinct and overlapping roles for AP-1 and GGAs revealed by the “knocksideways” system. *Curr. Biol.* **22**, 1711–1716.

Hirst J., Borner G. H. H., Edgar J., Hein M. Y., Mann M., Buchholz F., Antrobus R., Robinson M. S. (2013) Interaction between AP-5 and the hereditary spastic paraplegia proteins SPG11 and SPG15. *Mol. Biol. Cell* **24**, 2558–2569.

Hirst J., Itzhak D. N., Antrobus R., Borner G. H. H., Robinson M. S. (2018) Role of the AP-5 adaptor protein complex in late endosome-to-Golgi retrieval. *PLoS Biol.* **16**.

Hirst J., Madeo M., Smets K., Edgar J. R., Schols L., Li J., Yarrow A., et al. (2016) Complicated spastic paraplegia in patients with AP5Z1 mutations (SPG48). *Neurol. Genet.* **2**.

Hunter M. R., Hesketh G. G., Benedyk T. H., Gingras A. C., Graham S. C. (2018) Proteomic and Biochemical Comparison of the Cellular Interaction Partners of Human VPS33A and VPS33B. *J. Mol. Biol.* **430**, 2153–2163.

Jewell J. L., Russell R. C., Guan K. L. (2013) Amino acid signalling upstream of mTOR. *Nat. Rev. Mol. Cell Biol.* **14**, 133–139.

Kim B. Y., Krämer H., Yamamoto A., Kominami E., Kohsaka S., Akazawa C. (2001) Molecular Characterization of Mammalian Homologues of Class C Vps Proteins That Interact with Syntaxin-7. *J. Biol. Chem.* **276**, 29393–29402.

Lassmann T., Sonnhammer E. L. L. (2005) Kalign - An accurate and fast multiple sequence alignment algorithm. *BMC Bioinformatics* **6**.

Laufman O., Kedan A., Hong W., Lev S. (2009) Direct interaction between the COG complex and the SM protein, Sly1, is required for Golgi SNARE pairing. *EMBO J.* **28**, 2006–2017.

Martin E., Yanicostas C., Rastetter A., Naini S. M. A., Maouedj A., Kabashi E., Rivaud-Péchoux S., Brice A., Stevanin G., Soussi-Yanicostas N. (2012) Spatacsin and spastizin act in the same pathway required for proper spinal motor neuron axon outgrowth in zebrafish. *Neurobiol. Dis.* **48**, 299–308.

Mauvezin C., Ayala C., Braden C. R., Kim J., Neufeld T. P. (2014) Assays to monitor autophagy in Drosophila. *Methods* **68**, 134–139.

McLaughlin H. M., Sakaguchi R., Giblin W., Wilson T. E., Biesecker L., Lupski J. R., Talbot K., et al. (2012) A recurrent loss-of-function alanyl-tRNA synthetase (AARS) mutation in patients with charcot-marie-tooth disease type 2N (CMT2N). *Hum. Mutat.* **33**, 244–253.

Misura K. M. S., Scheller R. H., Weis W. I. (2000) *Three-dimensional structure of the*

neuronal-Sec1-syntaxin 1a complex.

Montecchiani C., Pedace L., Giudice T. Lo, Casella A., Mearini M., Gaudiello F., Pedroso J. L., et al. (2016) ALS5/SPG11/KIAA1840 mutations cause autosomal recessive axonal Charcot-Marie-Tooth disease. *Brain* **139**, 73–85.

Morrison H. A., Dionne H., Rusten T. E., Brech A., Fisher W. W., Pfeiffer B. D., Celniker S. E., Stenmark H., Bilder D. (2008) RegUlation of Early Endosomal Entry by the Drosophila tumor suppressors rabenosyn and Vps45. *Mol. Biol. Cell* **19**, 4167–4176.

Murmu R. P., Martin E., Rastetter A., Esteves T., Muriel M. P., Hachimi K. H. El, Denora P. S., et al. (2011) Cellular distribution and subcellular localization of spatacsin and spastizin, two proteins involved in hereditary spastic paraplegia. *Mol. Cell. Neurosci.* **47**, 191–202.

Nielsen E., Christoforidis S., Uttenweiler-Joseph S., Miaczynska M., Dewitte F., Wilm M., Hoflack B., Zerial M. (2000) Rabenosyn-5, a novel Rab5 effector, is complexed with hVPS45 and recruited to endosomes through a FYVE finger domain. *J. Cell Biol.* **151**, 601–612.

Nogueira C., Erlmann P., Villeneuve J., Santos A. J. M., Martinez-Alonso E., Martínez-Menárguez J. Á., Malhotra V. (2014) SLY1 and syntaxin 18 specify a distinct pathway for procollagen VII export from the endoplasmic reticulum. *Elife* **2014**.

Orlacchio A., Babalini C., Borreca A., Patrono C., Massa R., Basaran S., Munhoz R. P., et al. (2010) SPATACSIN mutations cause autosomal recessive juvenile amyotrophic lateral sclerosis. *Brain* **133**, 591–598.

Pensato V., Castellotti B., Gellera C., Pareyson D., Ciano C., Nanetti L., Salsano E., et al. (2014) Overlapping phenotypes in complex spastic paraplegias SPG11, SPG15, SPG35 and SPG48. *Brain* **137**, 1907–1920.

Pérez-Brangulí F., Mishra H. K., Prots I., Havlicek S., Kohl Z., Saul D., Rummel C., et al. (2014) Dysfunction of spatacsin leads to axonal pathology in SPG11-linked hereditary spastic paraplegia. *Hum. Mol. Genet.* **23**, 4859–4874.

Pulipparacharuvil S., Akbar M. A., Ray S., Sevrioukov E. A., Haberman A. S., Rohrer J., Krämer H. (2005) Drosophila Vps16A is required for trafficking to lysosomes and biogenesis of pigment granules. *J. Cell Sci.* **118**, 3663–3673.

Renvoisé B., Chang J., Singh R., Yonekawa S., FitzGibbon E. J., Mankodi A., Vanderver A., et al. (2014) Lysosomal abnormalities in hereditary spastic paraplegia types SPG15 and SPG11. *Ann. Clin. Transl. Neurol.* **1**, 379–389.

Rohrer J., Schweizer A., Russell D., Kornfeld S. (1996) The targeting of lamp1 to lysosomes is dependent on the spacing of its cytoplasmic tail tyrosine sorting motif relative to the membrane. *J. Cell Biol.* **132**, 565–576.

Schneider I. (1972) Cell lines derived from late embryonic stages of Drosophila melanogaster. *J. Embryol. Exp. Morphol.* **27**, 353–365.

Schröder B., Wrocklage C., Pan C., Jäger R., Kösters B., Schäfer H., Elsässer H. P., Mann M., Hasilik A. (2007) Integral and associated lysosomal membrane proteins. *Traffic* **8**, 1676–1686.

Słabicki M., Theis M., Krastev D. B., Samsonov S., Mundwiller E., Junqueira M., Paszkowski-Rogacz M., et al. (2010) A genome-scale DNA repair RNAi screen identifies SPG48 as a novel gene associated with hereditary spastic paraplegia. *PLoS Biol.* **8**.

Söding J., Biegert A., Lupas A. N. (2005) The HHpred interactive server for protein homology detection and structure prediction. *Nucleic Acids Res.* **33**.

Solinger J. A., Spang A. (2013) *Tethering complexes in the endocytic pathway: CORVET*

and HOPS.

Stepensky P., Saada A., Cowan M., Tabib A., Fischer U., Berkun Y., Saleh H., et al. (2013) The Thr224Asn mutation in the VPS45 gene is associated with the congenital neutropenia and primary myelofibrosis of infancy. *Blood* **121**, 5078–5087.

Stevanin G., Santorelli F. M., Azzedine H., Coutinho P., Chomilier J., Denora P. S., Martin E., et al. (2007) Mutations in SPG11, encoding spatacsin, are a major cause of spastic paraplegia with thin corpus callosum. *Nat. Genet.* **39**, 366–372.

Swairjo M. A., Otero F. J., Yang X. L., Lovato M. A., Skene R. J., McRee D. E., Pouplana L. R. De, Schimmel P. (2004) Alanyl-tRNA synthetase crystal structure and design for acceptor-stem recognition. *Mol. Cell* **13**, 829–841.

Szymanski C. J., Humphries IV W. H., Payne C. K. (2011) Single particle tracking as a method to resolve differences in highly colocalized proteins. *Analyst* **136**, 3527–3533.

Timmerman V., Strickland A. V., Züchner S. (2014) *Genetics of Charcot-Marie-Tooth (CMT) disease within the frame of the human genome project success*.

Toonen R. F. G., Verhage M. (2003) *Vesicle trafficking: Pleasure and pain from SM genes*.

Urban D., Li N., Christensen H., Pluthero F. G., Chen S. Z., Puhacz M., Garg P. M., et al. (2012) The VPS33B-binding protein VPS16B is required in megakaryocyte and platelet α-granule biogenesis. *Blood* **120**, 5032–5040.

Vantaggiato C., Crimella C., Airoldi G., Polishchuk R., Bonato S., Brighina E., Scarlato M., et al. (2013) Defective autophagy in spastizin mutated patients with hereditary spastic paraparesis type 15. *Brain* **136**, 3119–3139.

Varga R. E., Khundadze M., Damme M., Nietzsche S., Hoffmann B., Stauber T., Koch N., et al. (2015) In Vivo Evidence for Lysosome Depletion and Impaired Autophagic Clearance in Hereditary Spastic Paraplegia Type SPG11. *PLoS Genet.* **11**.

Wallen R. C., Antonellis A. (2013) *To charge or not to charge: Mechanistic insights into neuropathy-associated tRNA synthetase mutations*.

Wartosch L., Günesdogan U., Graham S. C., Luzio J. P. (2015) Recruitment of VPS33A to HOPS by VPS16 Is Required for Lysosome Fusion with Endosomes and Autophagosomes. *Traffic* **16**, 727–742.

Webb B., Sali A. (2016) Comparative protein structure modeling using MODELLER. *Curr. Protoc. Bioinforma.* **2016**, 5.6.1-5.6.37.

Wei N., Zhang Q., Yang X. L. (2019) Neurodegenerative Charcot–Marie–Tooth disease as a case study to decipher novel functions of aminoacyl-tRNA synthetases. *J. Biol. Chem.* **294**, 5321–5339.

Weimer R. M., Richmond J. E. (2004) Synaptic Vesicle Docking: A Putative Role for the Munc18{plus 45 degree rule}Sec1 Protein Family. *Curr. Top. Dev. Biol.* **65**, 83–113.

Wu M. N., Littleton J. T., Bhat M. A., Prokop A., Bellen H. J. (1998) ROP, the Drosophila Sec1 homolog, interacts with syntaxin and regulates neurotransmitter release in a dosage-dependent manner. *EMBO J.* **17**, 127–139.

Yu L., McPhee C. K., Zheng L., Mardones G. A., Rong Y., Peng J., Mi N., et al. (2010) Termination of autophagy and reformation of lysosomes regulated by mTOR. *Nature* **465**, 942–946.

Zhao W., Zhu Q. Y., Zhang J. T., Liu H., Wang L. J., Chen Z. Q., Guan L. P., Huang X. S., Yang L., Yu S. Y. (2013) Exome sequencing identifies novel compound heterozygous mutations in SPG11 that cause autosomal recessive hereditary spastic paraplegia. *J. Neurol. Sci.* **335**, 112–117.

Zimmermann L., Stephens A., Nam S. Z., Rau D., Kübler J., Lozajic M., Gabler F., Söding J., Lupas A. N., Alva V. (2018) A Completely Reimplemented MPI Bioinformatics Toolkit with a New HHpred Server at its Core. *J. Mol. Biol.* **430**, 2237–2243.

Table 1. Top 100 unique hits found in mass spectrometry output from GFP::Spg11-C purification from PMT-GFP::Spg11-C. Biological process and human ortholog (Human Ortho) data are from Flybase (www.flybase.org). Some of the hits discussed in the text are in bold.

Gene	Protein	CDS	Score	Matches	Sequences	Biological Process	Cellular Component	Human Ortho
CG13531	**CG13531**	**PB**	**14611**	**290**	**17**	**axon extension**	**axon**	**SPG11**
CG11700	CG11700	PB	1876	82	5	protein ubiquitination	microtubule associated complex	RPS27A
deltaCOP	**CG14813**	**PA**	**1813**	**41**	**13**	**retrograde vesicle-mediated transport, Golgi to ER**	**COPI vesicle coat**	**ARCN1**
CG30109	CG30109	PB	1771	27	3	biological_process	cellular_component	TRIAP1
Cisd2	**CG1458**	**PA**	**1630**	**28**	**3**	**biological_process**	**intracellular membrane-bounded organelle**	**CISD2**
Prx2540-2	CG11765	PA	1604	51	11	cell redox homeostasis	cytosol	PRDX6
Prx2540-1	CG12405	PA	1430	47	10	hydrogen peroxide catabolic process	cytosol	PRDX6
CG12896	CG12896	PA	1193	40	9	mesoderm development	cytoplasm	PRDX6
Dgp-1	CG5729	PA	1192	25	10	biological_process	cellular_component	GTPBP1
Rep	CG8432	PA	1192	25	8	neurotransmitter secretion	Rab-protein geranylgeranyltransferase complex	CHM
MetRS	**CG15100**	**PA**	**1147**	**26**	**14**	**methionyl-tRNA aminoacylation**	**microtubule associated complex**	**MARS**
Aldh-III	CG11140	PE	1087	25	10	oxidation-reduction process	lipid particle	GK5
Prosalpha 2	CG5266	PA	1053	21	5	proteasome-mediated ubiquitin-dependent protein catabolic process	proteasome core complex	PSMA7
mys	CG1560	PA	969	23	7	central nervous system development	focal adhesion	ITGB8
mys	CG1560	PB	916	21	6	central nervous system development	focal adhesion	ITGB8
su(r)	CG2194	PC	913	18	11	'de novo' pyrimidine nucleobase biosynthetic process	cytoplasm	DPYD
eEF1delta	CG4912	PA	892	16	5	translational elongation	eukaryotic translation elongation factor 1 complex	EEF1D
Msp300	CG42768	PG	797	18	15	mesoderm development	actin cytoskeleton	SYNE2
Msp300	CG42768	PD	796	17	14	mesoderm development	actin cytoskeleton	SYNE2
Hsp27	CG4466	PA	794	14	3	determination of adult lifespan	microtubule associated complex	HSPB6
eIF4G	CG10811	PA	741	19	13	translational initiation	cytosol	EIF4G1
smid	CG8571	PA	710	11	5	neurogenesis	-	NVL
Usp14	CG5384	PA	700	10	5	ubiquitin-dependent protein catabolic process	microtubule associated complex	USP14
Prosalpha 3	CG9327	PA	682	16	5	ubiquitin-dependent protein catabolic process	cytoplasm	PSMA4
CG8005	CG8005	PA	675	16	6	peptidyl-lysine modification to peptidyl-hypusine	-	DHPS
r	CG18572	PA	652	17	12	'de novo' pyrimidine nucleobase biosynthetic process	cytoplasm	CPS1
CG17514	CG17514	PA	651	18	13	regulation of translation	-	GCN1
Tango7	**CG8309**	**PA**	**632**	**15**	**7**	**Golgi organization**	**Golgi apparatus**	**EIF3M**
Rpn5	CG1100	PA	627	19	9	proteasome-mediated ubiquitin-dependent protein catabolic process	proteasome regulatory particle	PSMD12
nop5	CG10206	PA	605	12	7	rRNA processing	nucleolus	NOP58
Ts	CG3181	PA	591	7	3	deoxyribonucleotide biosynthetic process	-	TYMS
Cp1	CG6692	PA	590	15	4	protein catabolic process	lysosome	CTSS
Mrp4	CG14709	PB	588	13	9	drug transmembrane transport	ATP-binding cassette (ABC) transporter complex	ABCC4
Dhc64C	**CG7507**	**PA**	**582**	**14**	**11**	**cellularization**	**cytoplasm**	**DYNC1H1**
rhea	CG6831	PB	526	13	9	cytoskeletal anchoring at plasma membrane	focal adhesion	TLN2

CG7945	CG7945	PA	524	9	5	protein folding	-	BAG2
poe	CG14472	PA	519	15	12	spermatid development	P granule	UBR4
CG7945	CG7945	PB	510	8	4	protein folding	-	BAG2
msk	CG7935	PA	475	10	6	protein import into nucleus	cytoplasm	IPO7
CG10289	CG10289	PA	474	9	7	-	-	
ade5	CG3989	PA	461	11	6	inter-male aggressive behavior	cytoplasm	PAICS
hts	CG43443	PA	452	8	5	axon guidance	lipid particle	
Rpt6R	CG2241	PA	440	14	5	neurogenesis	microtubule associated complex	PSMC2
Prosalpha 4	CG3422	PA	434	10	4	cellular response to DNA damage stimulus	microtubule associated complex	PSMA7
Rpn7	CG5378	PA	420	10	4	proteolysis	proteasome regulatory particle, lid subcomplex	PSMD6
pic	CG7769	PA	418	16	6	positive regulation of protein catabolic process	nucleus	DDB1
Cand1	CG5366	PA	415	6	3	regulation of protein stability	-	CAND1
Prosalpha 6	CG4904	PB	409	12	6	proteasome-mediated ubiquitin-dependent protein catabolic process	cytoplasm	PSMA1
FKBP59	CG4535	PA	402	12	6	peripheral nervous system development	inaD signaling complex	FKBP5
kcc	CG5594	PE	391	8	5	transport	integral component of membrane	SLC12A5
eIF-2beta	CG4153	PA	388	7	2	translational initiation	cytosol	EIF2S2
Uch-L5	CG3431	PA	382	12	5	protein deubiquitination	proteasome regulatory particle	UCHL5
Rab35	**CG9575**	**PA**	**379**	**12**	**3**	**mitotic cytokinesis**	**lipid particle**	**RAB8B**
Int6	CG9677	PA	376	9	5	translational initiation	eukaryotic translation initiation factor 3 complex	EIF3E
CG31918	CG31918	PA	375	10	6	proteolysis	-	PHEX
Mfe2	CG3415	PA	368	7	4	fatty acid beta-oxidation using acyl-CoA oxidase	peroxisome	HSD17B4
ND-75	CG2286	PA	362	10	8	cellular respiration	mitochondrial respiratory chain complex I	NDUFS1
Pect	CG5547	PB	362	12	7	ethanolamine-containing compound metabolic process	-	PCYT2
MAPk-Ak2	CG3086	PB	360	9	4	protein phosphorylation	cytoplasm	MAPKAPK5
Prosalpha 7	CG1519	PA	358	11	6	cellular response to DNA damage stimulus	microtubule associated complex	PSMA3
l(1)G0193	CG2206	PA	355	7	6	biological_process	cellular_component	
Ugt	CG6850	PA	348	4	4	protein glycosylation	cytoplasm	UGGT1
Rab4	**CG4921**	**PB**	**347**	**8**	**2**	**ovarian follicle cell-cell adhesion**	**synapse**	**RAB4B**
MtnA	CG9470	PA	346	10	2	response to metal ion	cellular_component	
CG10527	CG10527	PA	344	11	4	-	cytoplasm	
grsm	CG7340	PB	344	7	4	proteolysis	cytoplasm	NPEPL1
kcc	CG5594	PC	343	6	4	transport	integral component of membrane	SLC12A5
UQCR-14	CG3560	PA	342	10	5	mitochondrial electron transport, ubiquinol to cytochrome c	mitochondrial respiratory chain complex III	UQCRB
SerRS	**CG17259**	**PA**	**341**	**6**	**4**	**seryl-tRNA aminoacylation**	**cytoplasm**	**SARS**
rump	CG9373	PA	340	9	3	anterior/posterior axis specification, embryo	nuclear chromatin	MYEF2
smt3	CG4494	PA	337	6	2	phagocytosis	nucleus	SUMO2
PpD3	CG8402	PB	330	5	3	protein dephosphorylation	nucleus	PPP5C
rush	**CG14782**	**PA**	**329**	**10**	**4**	**neuron projection morphogenesis**	**early endosome**	**PLEKHF1**
CG9674	CG9674	PA	323	8	6	oxidation-reduction process	-	FDXR
CG1598	CG1598	PA	320	6	3	-	-	ASNA1
CG32576	**CG32576**	**PA**	**320**	**3**	**1**	**vesicle-mediated transport**	**cellular_component**	**GOLT1B**
Cyp9c1	CG3616	PA	319	5	4	oxidation-reduction process	membrane	CYP4F12
Prosalpha 5	CG10938	PA	317	11	5	proteasome-mediated ubiquitin-dependent protein catabolic process	proteasome core complex, alpha-subunit complex	PSMA5
CkIalpha	CG2028	PB	315	6	3	DNA repair	cytoplasm	CSNK1A1L
Mi-2	CG8103	PA	307	5	3	negative regulation of cohesin loading	nucleus	CHD3

CG40045	CG40045	PA	305	8	2	protein polyubiquitination	cellular_component	CDC34
Rpn12	CG4157	PA	300	5	3	neurogenesis	proteasome regulatory particle	PSMD8
Sgt	CG5094	PA	297	9	5	neuromuscular synaptic transmission	cellular_component	SGTA
COX5B	CG11015	PA	296	8	2	mitochondrial electron transport, cytochrome c to oxygen	mitochondrion	COX5B
kcc	CG5594	PA	294	6	3	transport	integral component of membrane	SLC12A5
Prx3	CG5826	PA	294	9	5	cell redox homeostasis	mitochondrion	PRDX2
emb	CG13387	PA	292	8	5	protein export from nucleus	nuclear pore	XPO1
CG9391	CG9391	PA	291	5	3	dephosphorylation	cytoplasm	IMPA2
Sec22	**CG7359**	**PA**	**290**	**5**	**2**	**vesicle-mediated transport**	**transport vesicle**	**SEC22B**
sqh	**CG3595**	**PA**	**283**	**6**	**3**	**ovarian follicle cell development**	**unconventional myosin complex**	**MYL12B**
LKRSDH	CG7144	PA	281	6	5	regulation of histone methylation	-	AASS
Exo84	CG6095	PA	279	4	3	meiotic spindle organization	exocyst	EXOC8
FK506-bp1	CG6226	PA	278	6	2	protein folding	nucleus	PPID
Prosbeta1	CG8392	PA	278	8	3	cellular response to DNA damage stimulus	proteasome core complex	PSMB6
poly	CG9829	PA	277	3	2	oocyte microtubule cytoskeleton polarization	cellular_component	
Arpc5	CG9881	PA	270	8	5	cell morphogenesis	lamellipodium	ARPC5
CG1640	CG1640	PB	269	6	5	biosynthetic process	mitochondrion	GPT2
Rab35	**CG9575**	**PC**	**268**	**8**	**2**	**mitotic cytokinesis**	**lipid particle**	**RAB8B**
Ppt1	**CG12108**	**PA**	**267**	**9**	**4**	**macromolecule depalmitoylation**	**lysosome**	**PPT1**

Table 2. Top 100 unique hits found in mass spectrometry output from GFP::Spg11-C purification from Act-Spg11- C::GFP. Biological process and human ortholog (Human Ortho) data from Flybase (www.flybase.org). Some of the hits discussed in the text are in bold.

Gene	Protein	CDS	Score	Matches	Sequences	Biological Process	Cellular Component	Human Ortho
Mlc-c	**CG3201**	**PA**	**8379**	**178**	**11**	**actin filament-based movement**	**myosin complex**	**MYL6B**
sqh	**CG3595**	**PA**	**5723**	**117**	**8**	**ovarian follicle cell development**	**unconventional myosin complex**	**MYL12B**
Actn	CG4376	PA	4354	115	28	actin filament bundle assembly	focal adhesion	ACTN4
Gel	CG1106	PA	3844	103	23	phagocytosis	actin filament	AVIL
CG13531	**CG13531**	**PB**	**3373**	**81**	**13**	**axon extension**	**axon**	**SPG11**
Swip-1	CG10641	PA	2215	43	9	mesoderm development	muscle tendon junction	EFHD1
cpb	CG17158	PA	1892	39	10	microtubule-based movement	dynactin complex	CAPZB
cpa	CG10540	PA	1701	44	9	actin filament organization	dynactin complex	CAPZA1
Arp3	CG7558	PA	1452	35	11	actin cytoskeleton organization	actin filament	ACTR3
didum	CG2146	PA	1215	28	13	anterior/posterior axis specification, embryo	myosin complex	MYO5B
Arpc2	CG10954	PA	1171	43	6	lateral inhibition	Arp2/3 protein complex	ARPC2
didum	CG2146	PB	931	23	11	anterior/posterior axis specification, embryo	myosin complex	MYO5B
CG15099	CG15099	PA	882	15	3			DOPEY2
Arp53D	CG5409	PB	829	40	2	cytoskeleton organization	actin filament	ACTBL2
Cisd2	**CG1458**	**PA**	**801**	**17**	**3**		**intracellular membrane-bounded organelle**	**CISD2**
msk	CG7935	PA	775	12	5	protein import into nucleus	cytoplasm	IPO7
Arpc1	CG8978	PB	772	22	9	actin filament polymerization	Arp2/3 protein complex	ARPC1B
Arpc3A	CG4560	PC	690	13	4	Arp2/3 complex-mediated actin nucleation	Arp2/3 protein complex	ARPC3
CG6707	**CG6707**	**PA**	**540**	**19**	**4**	**phosphatidylinositol dephosphorylation**	**lysosomal membrane**	**TMEM55B**
Hmt-1	CG4225	PA	534	8	2	heme transport	ATP-binding cassette (ABC) transporter complex	ABCB7
ck	CG7595	PA	507	11	6	sensory perception of sound	unconventional myosin complex	MYO7B
CG32521	CG32521	PA	446	7	2	-	-	
tmod	CG1539	PA	442	11	5	cytoskeleton organization	fusome	
mon2	CG8683	PB	391	10	6	pole plasm protein localization	endosome	MON2
eIF4G	CG10811	PA	384	6	3	translational initiation	cytosol	EIF4G1
CG4042	CG4042	PA	380	24	1	-	-	ATP5SL
Gie	**CG7891**	**PA**	**380**	**6**	**2**	**sister chromatid segregation**	**lysosome**	**ARL8B**
CG8578	CG8578	PA	348	6	4	adult somatic muscle development	-	LRRFIP1
CG32521	CG32521	PG	338	4	1	-	-	
AlaRS	**CG13391**	**PB**	**338**	**5**	**2**	**alanyl-tRNA aminoacylation**	**cytoplasm**	**AARS**
ValRS	**CG4062**	**PB**	**331**	**5**	**3**	**valyl-tRNA aminoacylation**	**cytoplasm**	**VARS**
CG7806	CG7806	PA	313	8	4	transmembrane transport	integral component of membrane	ABCC4
Cp1	CG6692	PA	303	7	2	protein catabolic process	lysosome	CTSS
Aldh-III	CG11140	PE	285	6	3	oxidation-reduction process	lipid particle	GK5
FASN1	CG3523	PA	285	5	5	triglyceride biosynthetic process	lipid particle	FASN
Arpc5	CG9881	PA	278	7	1	cell morphogenesis	lamellipodium	ARPC5
CG4552	CG4552	PA	276	4	2	border follicle cell migration	-	TBC1D23
jar	CG5695	PB	271	8	4	membrane organization	unconventional myosin complex	MYO6
Pp1-87B	CG5650	PA	262	4	2	protein dephosphorylation	protein phosphatase type 1 complex	PPP1CC
CG31729	CG31729	PA	238	5	2	phospholipid translocation	integral component of membrane	ATP9B
pav	**CG1258**	**PA**	**228**	**5**	**4**	**neurogenesis**	**kinesin complex**	**KIF23**

CG17272	CG17272	PA	226	3	2	-	-	
r	CG18572	PA	225	6	2	'de novo' pyrimidine nucleobase biosynthetic process	cytoplasm	CPS1
Tango7	**CG8309**	**PA**	**220**	**3**	**1**	**Golgi organization**	**Golgi apparatus**	**EIF3M**
RhoGDI	CG7823	PA	211	7	2	-	cytoplasm	ARHGDIA
Cand1	CG5366	PA	207	2	2	regulation of protein stability	-	CAND1
PRL-1	CG4993	PA	206	3	2	protein dephosphorylation	cytoplasm	PTP4A2
Rack1	CG7111	PA	206	7	3	oviposition	cytoplasm	GNB2L1
Snx1	**CG2774**	**PA**	**205**	**5**	**1**	**intracellular protein transport**	**retromer, tubulation complex**	**SNX1**
CG11334	CG11334	PA	202	5	1	translation	eukaryotic translation initiation factor 2B complex	MRI1
Rab39	**CG12156**	**PA**	**198**	**7**	**2**	**Rab protein signal transduction**	**Golgi apparatus**	**RAB39A**
Arp2	CG9901	PA	194	6	3	cytoskeleton organization	actin filament	ACTR2
RabX4	**CG31118**	**PA**	**179**	**6**	**1**	**Rab protein signal transduction**	**synapse**	**RAB10**
Arpc4	CG5972	PA	177	6	4	cell projection assembly	Arp2/3 protein complex	ARPC4
Iva	**CG6450**	**PC**	**177**	**4**	**2**	**cellularization**	**Golgi apparatus**	**CEP250**
FK506-bp1	CG6226	PA	176	7	4	protein folding	nucleus	PPID
rhea	CG6831	PB	172	2	2	cytoskeletal anchoring at plasma membrane	focal adhesion	TLN2
row	CG8092	PA	170	3	1	regulation of transcription, DNA-templated	protein complex	
Pgi	CG8251	PA	169	2	1	gluconeogenesis	lipid particle	GPI
Osbp	**CG6708**	**PA**	**167**	**2**	**2**	**sperm individualization**	**endoplasmic reticulum**	**OSBP2**
uex	CG42595	PE	162	5	2	cellular ion homeostasis	cellular_component	CNNM2
Hex-A	CG3001	PA	159	2	1	carbohydrate phosphorylation	-	HK2
msn	CG16973	PA	158	9	2	photoreceptor cell morphogenesis	cell cortex	TNIK
vimar	CG3572	PB	154	4	1	tricarboxylic acid cycle	plasma membrane	RAP1GDS1
Rack1	CG7111	PB	151	4	2	oviposition	cytoplasm	GNB2L1
Glt	CG9280	PA	150	1	1	synaptic target inhibition	basement membrane	
Rpn13	CG13349	PA	146	3	2	lateral inhibition	proteasome regulatory particle	ADRM1
CG9281	CG9281	PB	144	4	1	-	ATP-binding cassette (ABC) transporter complex	ABCF2
alien	CG9556	PA	141	1	1	protein stabilization	COP9 signalosome	
Dhc64C	**CG7507**	**PA**	**138**	**4**	**4**	**cellularization**	**cytoplasm**	**DYNC1H1**
CG7878	CG7878	PA	136	4	2	-	-	DDX53
Kap-alpha3	CG9423	PA	135	1	1	protein import into nucleus	nuclear pore	KPNA2
SerRS	**CG17259**	**PA**	**135**	**2**	**1**	**seryl-tRNA aminoacylation**	**cytoplasm**	**SARS**
Rme-8	**CG8014**	**PA**	**133**	**4**	**3**	**endocytosis**	**microtubule associated complex**	**DNAJC13**
Pp1-Y2	CG40448	PB	131	2	1	protein dephosphorylation	nucleus	PPP1CC
Gbeta13F	CG10545	PB	129	2	1	actin filament organization	heterotrimeric G-protein complex	GNB4
CG5482	CG5482	PA	129	2	1	protein folding	endomembrane system	FKBP8
Imp	CG1691	PC	126	2	1	nervous system development	precatalytic spliceosome	IGF2BP3
Stam	CG6521	PA	125	3	1	JAK-STAT cascade	ESCRT-0 complex	STAM2
MetRS	**CG15100**	**PA**	**125**	**1**	**1**	**methionyl-tRNA aminoacylation**	**microtubule associated complex**	**MARS**
CG12065	CG12065	PA	124	2	1	lateral inhibition	-	
SPARC	CG6378	PA	123	2	1	cell adhesion	basement membrane	SPARCL1
Gdi	**CG4422**	**PA**	**119**	**2**	**2**	**neurotransmitter secretion**	**synaptic vesicle**	**GDI2**
Mrp4	CG14709	PB	118	1	1	drug transmembrane transport	ATP-binding cassette (ABC) transporter complex	ABCC4
CG9044	CG9044	PB	118	1	1	protein localization	cytoplasm	STK11IP
msn	CG16973	PB	117	8	1	photoreceptor cell morphogenesis	cell cortex	TNIK
Flo2	CG32593	PF	117	2	2	cell adhesion	flotillin complex	FLOT2

CG10425	CG10425	PA	116	1	1	-	-	KDSR
raptor	**CG4320**	**PB**	**114**	**3**	**2**	**positive regulation of protein phosphorylation**	**TORC1 complex**	**RPTOR**
shot	CG18076	PA	114	1	1	muscle attachment	fusome	SMTN
Flo2	CG32593	PC	107	1	1	cell adhesion	flotillin complex	FLOT2
Cyp9c1	CG3616	PA	107	1	1	oxidation-reduction process	membrane	CYP4F12
Klp61F	**CG9191**	**PA**	**105**	**2**	**2**	**neurogenesis**	**cytoplasm**	**KIF11**
PpD3	CG8402	PB	103	3	1	protein dephosphorylation	nucleus	PPP5C
blp	CG5268	PA	101	1	1	embryonic development via the syncytial blastoderm	cellular_component	PAM16
CG8336	CG8336	PB	99	6	1	protein folding	-	PPID
CG3587	CG3587	PA	98	2	1	-	-	KTI12
CG30122	CG30122	PB	98	1	1	mRNA splicing, via spliceosome	precatalytic spliceosome	
Vps35	**CG5625**	**PA**	**98**	**1**	**1**	**vesicle-mediated transport**	**endosome**	**VPS35**

Table 3. Protein hits identified from GFP::Spg11-C purification from both Act5-GFP::Spg11-C and PMT-GFP::Spg11-C. Proteins are ranked by highest score present in either of the two lines. Proteins mentioned in the text are highlighted. Human orthologue (Human Orth) data are from Flybase (www.flybase.org). Some of the hits discussed in the text are in bold.

#	Protein	Gene	Human Orth	#	Protein	Gene	Human Orth	#	Protein	Gene	Human Orth
1	**CG13531**	***CG13531***	**SPG11**	**51**	**CG15811**	***Rop***	**STXBP3**	**101**	CG1828	*dre4*	SUPT16H
2	CG5409	*Arp53D*	ACTBL2	**52**	CG13849	*Nop56*	NOP58	**102**	CG7207	*cert*	COL4A3BP
3	CG2241	*Rpt6R*	PSMC2	**53**	CG10990	*Pdcd4*	PDCD4	**103**	CG6020	*ND-39*	ENS G00000255639
4	CG7878	*CG7878*	DDX53	**54**	CG5650	*Pp1-87B*	PPP1CC	**104**	CG5336	*Ced-12*	ELMO3
5	CG1458	*Cisd2*	CISD2	**55**	CG3523	*FASN1*	FASN	**105**	CG1484	*flil*	FLII
6	CG11765	*Prx2540-2*	PRDX6	**56**	CG5504	*l(2)tid*	DNAJA3	**106**	CG4993	*PRL-1*	PTP4A2
7	**CG12156**	***Rab39***	**RAB39A**	**57**	CG3991	*TppII*	TPP2	**107**	CG4042	*CG4042*	ATP5SL
8	**CG31118**	***RabX4***	**RAB10**	**58**	CG12400	*ND-B14.5B*		**108**	CG43398	*scrib*	SCRIB
9	CG5729	*Dgp-1*	GTPBP1	**59**	CG11804	*ced-6*	GULP1	**109**	**CG2774**	***Snx1***	**SNX1**
10	**CG15100**	***MetRS***	**MARS**	**60**	**CG3201**	***Mlc-c***	**MYL6B**	**110**	CG6963	*gish*	CSNK1G3
11	CG11140	*Aldh-III*	GK5	**61**	CG10539	*S6k*	RPS6KA3	**111**	CG12202	*NAA15-16*	NAA15
12	CG15871	*mRpL38*	MRPL38	**62**	**CG5625**	***Vps35***	**VPS35**	**112**	CG5482	*CG5482*	FKBP8
13	CG10811	*eIF4G*	EIF4G1	**63**	CG4931	*Sra-1*	CYFIP1	**113**	**CG6708**	***Osbp***	**OSBP2**
14	CG18572	*r*	CPS1	**64**	CG1987	*Rbp1-like*	SRSF3	**114**	CG17158	*cpb*	CAPZB
15	CG17514	*CG17514*	GCN1	**65**	CG18076	*shot*	SMTN	**115**	CG9186	*CG9186*	LDAH
16	**CG8309**	***Tango7***	**EIF3M**	**66**	CG32056	*scramb1*	PLSCR1	**116**	**CG6450**	***Iva***	**CEP250**
17	CG1100	*Rpn5*	PSMD12	**67**	CG30122	*CG30122*		**117**	CG8578	*CG8578*	LRRFIP1
18	CG10206	*nop5*	NOP58	**68**	CG7558	*Arp3*	ACTR3	**118**	CG7421	*Nopp140*	NOLC1
19	CG6692	*Cp1*	CTSS	**69**	CG7324	*CG7324*	TBC1D9	**119**	CG8207	*CG8207*	GMPPA
20	CG14709	*Mrp4*	ABCC4	**70**	**CG4062**	***ValRS***	**VARS**	**120**	CG30159	*CG30159*	
21	**CG7507**	***Dhc64C***	**DYNC1H1**	**71**	CG7111	*Rack1*	GNB2L1	**121**	CG7985	*CG7985*	HEXDC
22	CG6831	*rhea*	TLN2	**72**	**CG10506**	***GlnRS***	**QARS**	**122**	CG43947	*PsGEF*	
23	CG7935	*msk*	IPO7	**73**	CG8261	*Ggamma1*	GNG10	**123**	CG7035	*Cbp80*	NCBP1
24	CG43443	*hts*		**74**	CG3585	*Rbcn-3A*	DMXL1	**124**	CG5268	*blp*	PAM16
25	CG5366	*Cand1*	CAND1	**75**	CG32138	*Frl*	DAAM2	**125**	CG8989	*His3.3B*	HIST1H3B
26	CG5594	*kcc*	SLC12A5	**76**	CG4422	*Gdi*	GDI2	**126**	CG7538	*Mcm2*	MCM2
27	CG3431	*Uch-L5*	UCHL5	**77**	CG3299	*Vinc*	VCL	**127**	**CG6707**	***CG6707***	**TMEM55B**
28	**CG17259**	***SerRS***	**SARS**	**78**	CG9423	*Kap-alpha3*	KPNA2	**128**	**CG4320**	***raptor***	**RPTOR**
29	CG8402	*PpD3*	PPP5C	**79**	CG10545	*Gbeta13F*	GNB4				
30	CG3616	*Cyp9c1*	CYP4F12	**80**	CG10913	*Spn55B*	SERPINB2				
31	CG5094	*Sgt*	SGTA	**81**	CG4265	*Uch*	UCHL3				
32	CG11015	*COX5B*	COX5B	**82**	CG3001	*Hex-A*	HK2				
33	**CG3595**	***sqh***	**MYL12B**	**83**	**CG8014**	***Rme-8***	**DNAJC13**				
34	CG6226	*FK506-bp1*	PPID	**84**	CG8683	*mon2*	MON2				
35	CG9881	*Arpc5*	ARPC5	**85**	CG17950	*HmgD*	SSRP1				
36	CG12108	*Ppt1*	PPT1	**86**	CG8284	*Ubc4*	UBE2K				
37	CG7619	*Rpn10*	PIP5K1C	**87**	CG12918	*sel*	CNPY1				
38	CG9281	*CG9281*	ABCF2	**88**	CG5252	*Ranbp9*	IPO9				
39	CG10425	*CG10425*	KDSR	**89**	CG8487	*garz*	GBF1				
40	CG13349	*Rpn13*	ADRM1	**90**	CG12132	*c11.1*	MROH7				
41	CG3226	*CG3226*	CACYBP	**91**	CG12065	*CG12065*					
42	CG34373	*Sarm*	SARM1	**92**	CG4225	*Hmt-1*	ABCB7				
43	CG16973	*msn*	TNIK	**93**	CG10161	*eIF-3p66*	EIF3D				
44	CG8251	*Pgi*	GPI	**94**	CG14616	*l(1)G0196*	PPIP5K1				
45	CG9242	*bur*	GMPS	**95**	CG42595	*uex*	CNNM2				
46	**CG13391**	***AlaRS***	**AARS**	**96**	CG3572	*vimar*	RAP1GDS1				
47	CG1691	*Imp*	IGF2BP3	**97**	CG11334	*CG11334*	MRI1				
48	CG6783	*fabp*	FABP2	**98**	CG4560	*Arpc3A*	ARPC3				
49	CG3593	*r-l*	UMPS	**99**	CG7806	*CG7806*	ABCC4				
50	**CG7891**	***Gie***	**ARL8B**	**100**	CG8715	*lig*	UBAP2				

Table 4. Enrichment analysis for Spg11 C-terminal interactors identified in both constitutive and inducible interaction screens.

Enrichment analysis is shown for human orthologs. GO terms with large gene sets (>2000) and smaller sets with less specific terms are omitted. Full lists are in Supplementary Information.

GO-term	Molecular Function	Count in gene set	False Discovery Rate
GO:0008144	drug binding	32 of 1710	2.97E-06
GO:0005524	ATP binding	29 of 1462	2.97E-06
GO:0004812	aminoacyl-tRNA ligase activity	5 of 43	0.00032
GO:0003723	RNA binding	17 of 850	0.00049
GO:0140296	general transcription initiation factor binding	4 of 39	0.00300
GO:0045182	translation regulator activity	6 of 124	0.00300
GO:0003779	actin binding	10 of 413	0.00470
GO-term	**Biological Process**		
GO:0006897	vesicle-mediated transport	30 of 1699	0.00022
GO:0016192	regulated exocytosis	17 of 691	0.00043
GO:0051234	neutrophil degranulation	14 of 485	0.00060
GO:0043604	phagocytosis	9 of 185	0.00063
GO:0006810	endocytosis	14 of 510	0.00063
GO:0045055	translation	12 of 362	0.00063
GO:0043312	cell activation involved in immune response	15 of 620	0.00075
GO:1901566	secretion	20 of 1070	0.00086
GO:0006909	membrane organization	16 of 729	0.00110
KEGG Pathway	**Description**		
dme00970	Aminoacyl-tRNA biosynthesis	5 of 42	0.0031
dme04144	Endocytosis	6 of 119	0.0236
dme03050	Proteasome	4 of 51	0.0236
dme02010	ABC transporters	3 of 22	0.0236

Table 5. Amino-acyl tRNA synthetase mass spectrometry results

		PMT-GFP::Spg11-C			
***Drosophila* Protein**	**Human Ortholog**	**CDS**	**Score**	**Matches**	**Sequences**
MetRS	MARS	PA	1147	26	14
SerRS	SARS	PA	341	6	4
AlaRS	AARS	PB	338	5	2
ValRS	VARS	PB	331	5	3
GlnRS	QARS	PA	125	4	3

Table 6. Members of the Sec1/Munc18 (SM) gene family in *Drosophila*

Gene Symbol	Gene Name	Also known as
car	*carnation*	*Vps33, Vps33a, l(1)G0447*
Rop	*Ras opposite*	*l(3)64Ah, cs1, Sec1, Munc18*
Slh	*SLY-1 homologous*	*Sly1, d-sly*
Vps33B	*Vacuolar protein sorting 33B*	
Vps45	*Vacuolar protein sorting 45*	*MEME(3R)-C*

Table 7. Rop, Vps45, Slh and Spg15 mass spectrometry score results

		PMT-GFP::Spg11-C			
Gene Symbol	**Protein**	**CDS**	**Score**	**Matches**	**Sequences**
Rop	CG15811	PA	180	3	3
Vps45	CG8228	PA	122	2	2
Slh	CG3539	PC	90	2	2